Available online at www.sciencedirect.com
SCIENCE DIRECT
International Journal of Heat and Mass Transfer 49 (2006) 601–610
International Journal of HEAT and MASS TRANSFER
www.elsevier.com/locate/ijhmt

Modeling for shell-side pressure drop for liquid flow in shell-and-tube heat exchanger

Uday C. Kapale, Satish Chand *

Department of Mechanical Engineering, Motilal Nehru National Institute of Technology, Deemed University, Allahabad 211 004, India

Received 27 December 2004; received in revised form 18 July 2005
Available online 2 November 2005

Abstract

A theoretical model for shell-side pressure drop has been developed. The model incorporates the effect of pressure drop in inlet and outlet nozzles along with the losses in the segments created by baffles. The results of the model for Reynolds numbers lying between 10^3 and 10^5 match more closely with the experimental results available in the literature compared to analytical models developed by other researchers for different configurations of heat exchangers.

Keywords: Cross flow velocities; Pressure drop; Segmental baffles; Shell-and-tube heat exchanger; Shell-side flow; Window zone velocity

1. Introduction

The applications of single-phase shell-and-tube heat exchangers are quite large because these are widely used in chemical, petroleum, power generation and process industries. In these heat exchangers, one fluid flows through tubes while the other fluid flows in the shell across the tube bundle. The design of a heat exchanger requires a balanced approach between the thermal design and pressure drop. The pressure drop results in the increase of the operating cost of fluid moving devices such as pumps and fans. This shows that along with the design for the capacity for heat transfer, the pressure drop determinations across the heat exchanger are equally important. The estimations for pressure loss for the fluids flowing inside the tubes are relatively simple, but complex in the shell-side flow.

To evaluate the pressure drop in the shell, there is a need to know the various internal flow paths and their individual effects. Based on Tinker and Buffalo [2] flow stream analysis it can be seen in Fig. 1 that in addition to cross flow stream 'B' through the tube bundle from one baffle window to the next, there is a bypass stream 'C' which evades tube bundle and passes between the bundle and shell making no contribution to heat transfer. There is a further bypass stream 'D' which leaks through the clearance space between the baffles and shell, and leakage path 'A' through clearance spaces between the tubes and baffles which later on interact with the main cross flow stream. Fig. 1 also shows the flow pattern across tube bundle and in the window section. However this flow is further shown in Fig. 4. The flow direction of the main stream relative to the tubes is different in the window section created by the baffle cut from that in interior cross-flow section existing between the segmental baffles. This requires the use of different approaches to compute the pressure drop in window section than the flow across the tube bundle (cross-flow section). Similarly in the end crosses, the flow across the tube bundle is different than interior cross-flow which also has to be taken into account.

The works available in the literature may be put in two categories—(i) experimental works and (ii) development of theoretical models. The experimental works done by various authors are reported in the references [3,7,9,16,17,21].

* Corresponding author. Tel.: +91 532 2445077/2540212; fax: +91 532 2445101.
E-mail addresses: uday_kapale@hotmail.com (U.C. Kapale), satishchand@rediffmail.com (S. Chand).

0017-9310/$ - see front matter © 2005 Elsevier Ltd. All rights reserved.
doi:10.1016/j.ijheatmasstransfer.2005.08.022

Nomenclature

A_{bm}	mean of interior cross flow area and window zone flow area, m^2
A_{sc}	interior cross flow section area at or near the shell centerline, m^2
A_{wz}	window zone flow area, m^2
B_c	baffle cut percentage
B_s	interior sections baffle spacing, m
B_{si}	inlet section baffle spacing, m
B_{so}	outlet section baffle spacing, m
C_f	correction factor used in friction factor Eq. (10b)
D_b	baffle diameter, m
D_c	diameter of circle passing through centers of outermost tubes in the shell, m
D_0	tube bundle diameter, m
D_s	shell inside diameter, m
d	tube outside diameter, m
f	fanning friction coefficient
f_b	correction factor for bundle bypass stream for pressure drop
f_l	correction factor for effect of baffle leakage for pressure drop
f_s	correction factor for unequal baffle spacing at end sections
L	vertical height of cross flow zone (Fig. 2), m
l	distance between end tube plates, m
N_b	number of baffles
N_c	number of tube rows in cross flow
N_w	number of tube rows in window section
N_{wt}	number of tubes in window section
P	tube pitch (Fig. 3), m
P_p	longitudinal tube pitch (Fig. 3), m
P_t	transverse tube pitch (Fig. 3), m
r_b	radius of stream bend passing through window section (Fig. 4), m
Re_s	shell-side fluid end and interior cross flow Reynolds number
$\dot{V}$	volume flow rate of shell-side fluid, m^3/s
u_n	fluid velocity in inlet and outlet nozzles $\left(\dot{V}/\frac{\pi}{4}d_n^2\right)$, m/s
u_{sc}	cross flow velocity at the end and interior cross flow sections at or near shell center line, m/s
u_{wz}	fluid velocity in window, m/s
Δp_c	interior cross flow section pressure drop, Pa
Δp_{ec}	end cross flow sections pressure drop, Pa
Δp_n	inlet and outlet nozzles pressure drop, Pa
Δp_s	total shell-side pressure drop, Pa
Δp_{wz}	window zone pressure drop at window, Pa

Greek symbols

α	angle corresponding to baffle edge (Fig. 6), degrees
α_c	angle in reference to circle passing through center of outermost tubes at baffle cut (Fig. 6), degrees
μ_s	viscosity of shell fluid at average temperature, $N\,s/m^2$
μ_{sw}	viscosity of shell fluid at wall temperature, $N\,s/m^2$
ρ_s	shell-side fluid density at average temperature, kg/m^3
ξ_n	nozzles pressure drop coefficient
θ	shell-side fluid stream inclination angle with the axis of hell (Fig. 2), degrees

Further the works reported in the form of modeling are given in references [1,2,4,6,8,11,12,14,15,18,20,22,23]. On review of these, it is noticed that the literature models reported in some of the works are quite complex for computation, while the others have considered few components of pressure drop and ignored the others. In the present work an effort has been made to develop the simple pressure loss model. The results of this are compared with

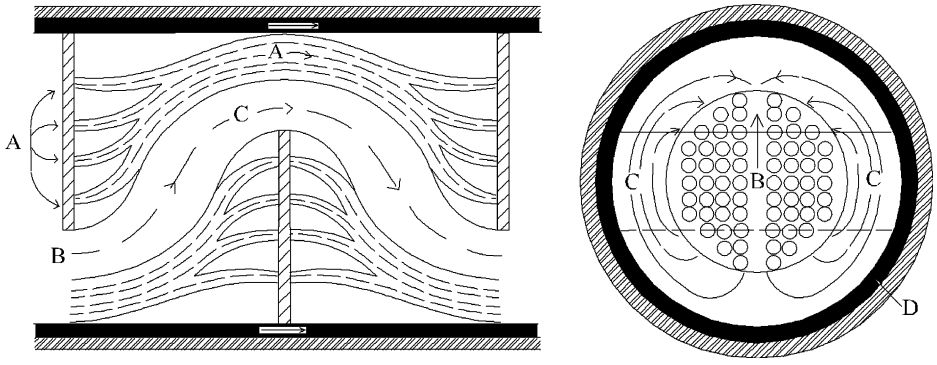

Fig. 1. Diagram indicating the flow streams in the shell.

the results available in the literature. The present model results are quite good and designers can use these confidently. The work is mainly concerned with liquid flows in the shell.

2. Pressure drop model development

The present work aims to determine the overall pressure loss in the shell from the point of entry of the fluid to the outlet point of fluid. The total pressure drop has been divided into the various components listed below:

(1) Pressure drop in the inlet and outlet nozzles at the end cross-sections of heat exchanger.
(2) The pressure drop in the interior cross sections. In these sections, the pressure loss is determined for the flow across the tube bundle and for the flow from interior section through window section to the next consecutive interior section.
(3) The pressure drop due to flow pattern in the inlet end cross-section across the tube bundle up to the level of baffle height and thereafter for the flow through window section. Similarly for the outlet end cross-section the pressure loss is first computed for the flow coming from the previous interior cross-section through window section and thereafter for the flow across the tube bundle.

The main contribution of the present work is concerned with developing the model to compute the pressure drop in the interior section and window section. For rest of the pressure drop components the expressions already available in the literature have been used.

The computation of the pressure drops across the tube bundle and through window section, efforts have been made to consider the actual flow pattern shown in Figs. 1 and 5. The pressure losses for each of the above components have been presented one by one in the following text of the paper.

2.1. Pressure drop in the inlet and outlet nozzles (Δp_n)

For computing the pressure drop in both inlet and outlet nozzles in an heat exchanger, the expression given in the research paper of Gaddis and Gnielinski [18] has been used and is given by Eq. (1). This pressure drop for both the nozzles together is designated by Δp_n.

$$\Delta p_n = \frac{\rho_s \xi_n u_n^2}{2} \tag{1}$$

As discussed in Ref. [18] ξ_n has been taken as 2.0 and Eq. (1) becomes Eq. (2).

$$\Delta p_n = \rho_s u_n^2 \tag{2}$$

2.2. Pressure drop in the interior compartments cross flow section (Δp_c)

To develop the model, the simplified flow pattern given in the work of Emerson [4], here shown in Fig. 2, has been considered. In this figure in interior compartment, cross flow has been taken inclined and in window section it is shown by horizontal line. In actual flow shown in Figs. 1 and 5, the flow in window section is in the form of a curve and not a straight line. The modeling for pressure loss under this section has been presented in two parts as given below:

(i) Pressure drop across the tube bundle,
(ii) Pressure drop in the window section.

These are presented in Sections 2.2.1 and 2.2.2, respectively.

2.2.1. Modeling for pressure drop across the tube bundle

To model pressure drop across the tube bundle, the beginning has been made using the pressure drop expression for the flow across tube bundle given by Bell [12], which is reproduced here by Eq. (3).

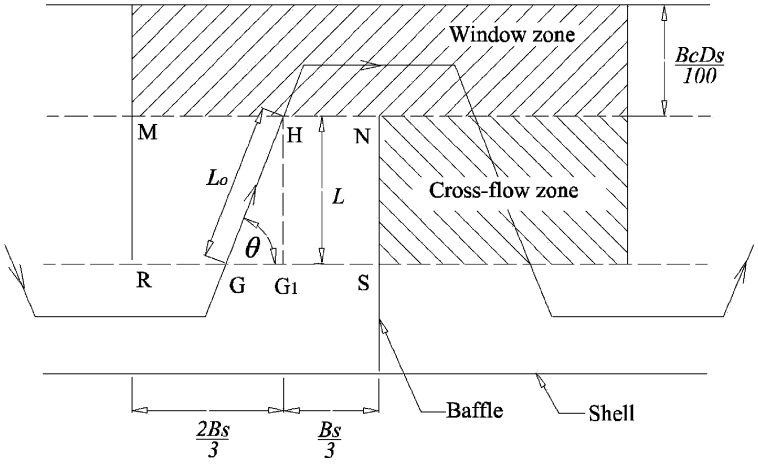

Fig. 2. Delination of cross-flow and window zones.

$$\Delta p_c = \frac{\rho_s f L u_{sc}^2}{2P_p} \tag{3}$$

In Eq. (3) given above, L has been determined assuming the vertical flow i.e. in G_1H direction as illustrated in Fig. 2. However, the actual flow direction is shown by GH line, which is inclined from horizontal by an angle θ. In the present work instead of flow direction G_1H has been approximated by GH (Fig. 2). The angle θ has been illustrated in the same diagram.

In view of the above, L in Eq. (3) has been replaced by GH, which has been taken equal to L_0. Substituting L_0 in place of L in Eq. (3), we get Eq. (4).

$$\Delta p_c = \frac{\rho_s f L_0 u_{sc}^2}{2P_p} \tag{4}$$

Referring to Fig. 2, we get $L_0 = \frac{L}{\sin\theta}$ and now making this substitution, Eq. (4) becomes Eq. (5).

$$\Delta p_c = \frac{\rho_s f u_{sc}^2}{2P_p} \frac{L}{\sin\theta} \tag{5}$$

As per the Ref. [8], substituting $N_c = \frac{L}{P_p}$ Eq. (5) becomes Eq. (6).

$$\Delta p_c = \frac{\rho_s f u_{sc}^2 N_c}{2\sin\theta} \tag{6}$$

2.2.1.1. Determination of θ. Refer to Fig. 2 and drop a perpendicular from H to G_1. Further MN and RS indicate baffle spacing. To determine θ, HN has been estimated as 1/3rd of baffle spacing and MH as 2/3rd of baffle spacing. The value of $\tan\theta$ is given by Eq. (7).

$$\tan\theta = \frac{HG_1}{GG_1} = \frac{L}{GG_1} = \frac{D_s\left(1-\frac{2B_c}{100}\right)}{\frac{B_s}{3}} = \frac{3D_s}{B_s}\left(1-\frac{2B_c}{100}\right) \tag{7}$$

This angle θ from Eq. (7) is used in Eq. (6).

2.2.1.2. Determination of cross flow velocity u_{sc}. The expression for cross flow velocity u_{sc} is given by Eq. (8).

$$u_{sc} = \frac{\dot{V}}{A_{sc}} \tag{8}$$

The expression for A_{sc} has been taken from Ref. [12] and given here by Eq. (9).

$$A_{sc} = B_s\left[(D_s - D_0) + \frac{(D_0 - d)(P - d)}{P_t}\right] \tag{9}$$

2.2.1.3. Determination of friction factor. In the present work, the overall objective is to give a simplified procedure for the determination of pressure loss in heat exchanger. On review of the literature [19] we find that heat exchangers are generally arranged in any one of the four configurations illustrated in Fig. 3. As given in the works of Bell [12], Gaddis [18] and works of Taborek presented in the textbook of Kakac [23], the procedure to determine the friction factors is quite lengthy and complicated. However,

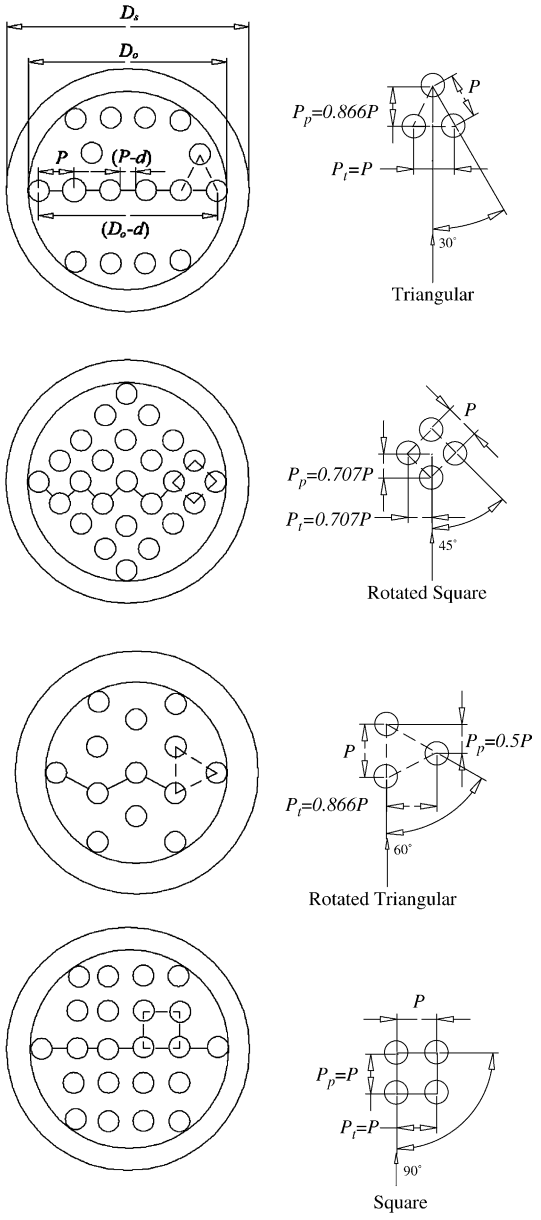

Fig. 3. Cross-flow areas at or near shell center line.

in the textbook of Kern [1] the friction factors are determined using the expression, which is a function of Reynolds number only and here given by Eq. (10a). But the results of Eq. (10a) do not match with the latest works reported in Refs. [12,18,23].

$$f = \exp(0.576 - 0.19\ln Re_s) \tag{10a}$$

In the present work initially the values of friction factors are determined using the works reported in references [18,23] for all the four configurations of tube bundles mentioned earlier and using these, the friction factor equation (10a) of Kern [1] has been modified for all the four configurations to develop the new empirical relation. This relation has been given here by Eq. (10b).

$$f = \exp(0.576 - 0.19\ln Re_s) + C_f \tag{10b}$$

Table 1
Friction correction factor (C_f)

Tube pitch/tube diameter (P/d)	Tube configuration							
	30°		45°		60°		90°	
	C_f for		C_f for		C_f for		C_f for	
	$Re_s < 10^4$	$Re_s > 10^4$	$Re_s < 10^4$	$Re_s > 10^4$	$Re_s < 10^4$	$Re_s > 10^4$	$Re_s < 10^4$	$Re_s > 10^4$
1.25	0.3752	0.1609	0.1355	0.0369	0.0601	−0.0136	0.0767	0.1578
1.33	0.2873	0.1296	0.0791	0.0280	0.0168	−0.0197	−0.0026	0.1129
1.50	0.1581	0.0854	−0.0119	0.1282	−0.0520	−0.0301	−0.1180	0.0428

The values of correction factor, C_f for different tube configurations and P/d values and Reynolds numbers are given in Table 1. Finally Eq. (10b) has been used to determine friction factors using the Reynolds number at various sections of heat exchanger.

To check the accuracy the values of friction factors computed from Eq. (10b) are compared with the friction factors obtained using the procedure of reference [18]. The comparison has been illustrated in Fig. 4 and the results of Eq. (10b) match within reasonable limits.

2.2.1.4. Consideration of leakage and bundle bypass factor. Bell [12] and Gaddis [18] have proposed that the pressure in the shell will also drop due to the leakages and bundle bypass of the fluid. The leakages of the fluid take place through the clearances between shell and baffle and also through the clearances between the holes in baffles and tube diameters. In addition the bypass stream C (Fig. 1) evades tube bundle and the shell. The effect of leakages and bundle bypass has been considered and Eq. (6) has been modified after multiplying it by leakage (f_l) and bypass factors (f_b) to get the final expression of Δp_c given by Eq. (11).

$$\Delta p_c = \frac{\rho_s f u_{sc}^2 N_c}{2 \sin\theta} f_l f_b \tag{11}$$

The values of f_l and f_b have been computed using the procedure given in Ref. [18]. Now pressure loss Δp_c given by Eq. (11) can be computed. However this equation is further modified for the fluids sensitive for the change in viscosity. For such fluids, the viscosities at bulk temperature and wall temperature are considered. Incorporating this effect the pressure loss model across the tube bundle is given by Eq. (12).

$$\Delta p_c = \frac{\rho_s f u_{sc}^2 N_c}{2 \sin\theta} f_l f_b \left(\frac{\mu_{sw}}{\mu_s}\right)^{0.14} \tag{12}$$

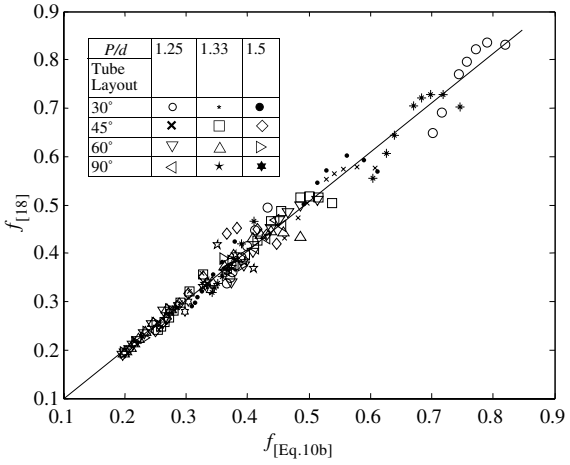

Fig. 4. Comparison of friction factors obtained by developed empirical relations with reference to Gaddis [18] method.

2.2.2. Pressure drop in window section zone (Δp_{wz})

To determine this pressure drop in the window zone the flow pattern shown in Fig. 5 has been taken into consideration. The pressure drop in the window zone is the summation of pressure drop due to convergent–divergent flow stream at window (Δp_{cdn}) and due to the bend formed by fluid stream (Δp_b). The flow from MN to PN has been considered as convergent flow and the flow from PN to NQ as divergent. The pressure loss for MN–PN–NQ flow has been determined considering it as convergent–divergent nozzle. The convergent and divergent parts of this nozzle are identical and therefore the pressure drop due to convergent nozzle is multiplied by 2, to determine the total drop in convergent–divergent nozzle. The pressure drop in convergent–divergent nozzle is given by Eq. (13a).

$$\Delta p_{cdn} = 2 \times \text{Pressure drop in convergent nozzle} \tag{13a}$$

The mathematical expression for convergent nozzle has been taken from the textbook [5] and after incorporating the leakage correction factor, f_l [8,12,18] Δp_{cdn} is given by Eq. (13b). In the window section zone, there is no effect of bundle bypass leakage and therefore ignored here.

$$\Delta p_{cdn} = \frac{2\rho_s u_{sc}^2 f_l}{2}\left[\left(\frac{A_{sc}}{A_{wz}}\right)^2 - 1\right]\left(\frac{\mu_{sw}}{\mu_s}\right)^{0.14} \tag{13b}$$

A_{wz} = window area excluding the area of tubes in window zone

Referring to Fig. 6 window area including tubes,

$$= \left\{\frac{\pi D_s^2}{4}\frac{\alpha}{360} - \left[\frac{D_s}{4}\left(1 - \frac{2B_c}{100}\right) D_b \sin\left(\frac{\alpha}{2}\right)\right]\right\} \tag{14}$$

$$\text{Area of window tubes} = N_{wt}\frac{\pi d^2}{4} \tag{15}$$

$$A_{wz} = \left\{\frac{\pi D_s^2}{4}\frac{\alpha}{360} - \left[\frac{D_s}{4}\left(1 - \frac{2B_c}{100}\right) D_b \sin\left(\frac{\alpha}{2}\right)\right] - N_{wt}\frac{\pi d^2}{4}\right\} \tag{16}$$

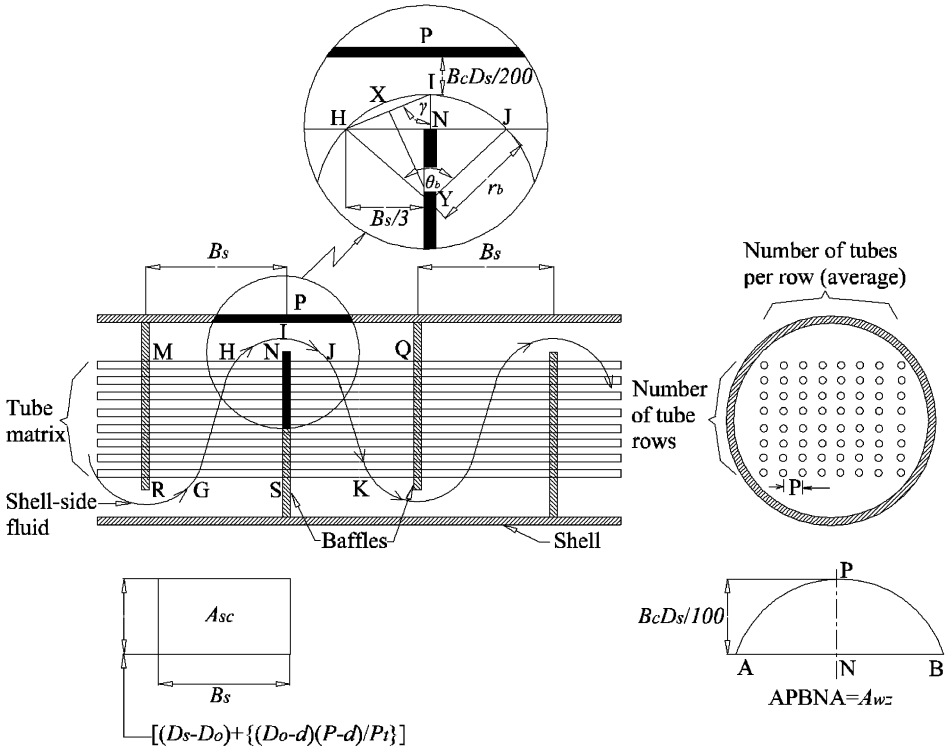

Fig. 5. Showing the actual flow pattern in shell-side.

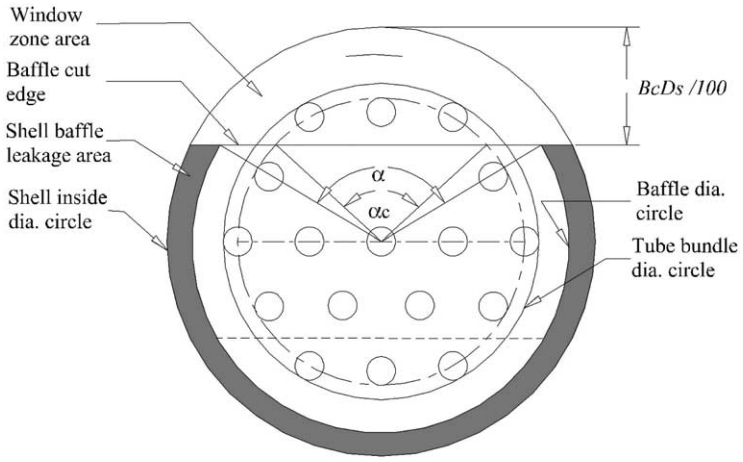

Fig. 6. Illustration of baffle cut angles, leakage area.

N_{wt} is determined using the expressions in Ref. [8]. In addition to the convergent–divergent nozzle, the pressure loss due to flow stream bend *HIJ* in window zone (Fig. 5) has been determined using the procedure given below.

2.2.2.1. Determination of pressure drop for flow stream bend HIJ in window zone. The geometry of bend has been shown in Fig. 5. The cross section of the bend is rectangular at inlet *MN* and segmental section at the center *NP*. At the inlet the cross-sectional area is larger, which has been assumed to converge uniformly in the form of segmental area at the window section. The geometry of bend at inlet *MN* and outlet *NQ* is same. In view of this the bend uniformly diverges from segmental area at window center *NP* to rectangular section at outlet *NQ*.

To simplify the problem the bend has been transformed into uniform cross-sectional area, which is the average of inlet area at *MN* and central area at *NP*. This average area has been further transformed to equivalent circular area. The procedure adopted for this transformation is discussed below:

(i) Actual inlet area of bend: This area is nothing but area A_{sc} given by Eq. (9).

(ii) Segmental area, A_{wz} of the bend at the center of window section: The segmental area at the center is given by Eq. (16).

(iii) The mean area of inlet and central area of bend: It is given by the Eq. (17).

$$A_{bm} = \frac{A_{sc} + A_{wz}}{2} \tag{17}$$

(iv) The diameter of flow stream bend (d_{bs}) in the window zone assumed of uniform circular cross-sectional area is given by the Eq. (18).

$$d_{bs} = \sqrt{\frac{2(A_{sc} + A_{wz})}{\pi}} \tag{18}$$

2.2.2.2. Determination of the radius of flow stream bend HIJ in the window zone. Using the geometry of bend given in the Fig. 5, considering the right angled triangle HNI and assuming $\angle HIN = \gamma$, further as per earlier discussions substituting $HN = B_s/3$ and $NI = B_c D_s/200$, the angle γ is given by Eqs. (19).

$$\tan\gamma = \frac{B_s/3}{B_c D_s/200} \quad \text{or} \tag{19a}$$

$$\gamma = \tan^{-1}\left(\frac{200 B_s}{3 B_c D_s}\right) \tag{19b}$$

Further, $\sin\gamma = \frac{HN}{HI} = \frac{B_s/3}{HI}$

$$\text{or} \quad HI = \frac{B_s}{3\sin\gamma} \tag{19c}$$

Now in Fig. 5 drop a perpendicular YX on the line HI from the center of flow stream bend Y. The point X is the center of HI. Now considering right angled triangle IXY, $\cos\gamma$ is given by Eq. (19d).

$$\cos\gamma = \frac{IX}{IY} = \frac{\frac{1}{2}HI}{IY} \tag{19d}$$

Substituting the value of HI from Eq. (19c),

$$IY = \frac{\frac{1}{2}\left(\frac{B_s}{3\sin\gamma}\right)}{\cos\gamma} = \frac{B_s}{3\sin 2\gamma} \tag{19e}$$

IY is nothing but the radius of flow stream bend (r_b) in window zone and substituting $IY = r_b$, we get Eq. (19f).

$$\text{Now } r_b = \frac{B_s}{3\sin 2\gamma} \tag{19f}$$

2.2.2.3. Determination of flow stream bend angle, θ_b in the window zone. Referring to Fig. 5 $\angle HYJ = \theta_b$ is the bend angle. Now considering right angled triangle HNY, we get Eqs. (20).

$$\sin\frac{\theta_b}{2} = \frac{HN}{HY} = \frac{B_s/3}{r_b} \quad \text{or} \tag{20a}$$

$$\theta_b = 2\sin^{-1}\left(\frac{B_s/3}{r_b}\right) \tag{20b}$$

2.2.2.4. Determination of pressure drop due to flow stream bend (Δp_b) in the window section. The procedure given in reference [10] has been followed to compute the pressure loss in a bend. According to this procedure Δp_b is expressed by Eqs. (21).

$$\Delta p_b = \frac{\rho_s k u_{wz}^2}{2} \tag{21a}$$

$$u_{wz} = \frac{\dot{V}}{A_{wz}} \tag{21b}$$

The procedure for determination of pressure drop coefficient k for $0.5 \leqslant R_b/d_b \leqslant 1.5$ is given below.

$$k = k_1 + k_2 \tag{21c}$$

As per the reference quoted above,

$$k_1 = A \times B \tag{21d}$$

$$k_2 = 0.17 f \frac{r_b}{d_{bs}} \tag{21e}$$

The values of friction factor, f are determined with the help of Eq. (10b) using Reynolds number for the flow velocity in window zone. To find out the constants A and B, graphs are given in reference [10]. A is dependent on flow stream bend angle θ_b and B is dependent on r_b/d_{bs} ratio. In the present work to avoid the use of graph, expressions have been developed for A and B using the regression analysis for curve fitting here and given by Eqs. (22).

$$\begin{aligned} A &= 0.0278\theta_b^{0.827} \quad \text{for } \theta_b \leqslant 50 \\ &= 0.0875\theta_b^{0.534} \quad \text{for } 50 \leqslant \theta_b \leqslant 180 \end{aligned} \tag{22a}$$

$$\begin{aligned} B &= 0.194\left(\frac{r_b}{d_{bs}}\right)^{-2.8} \quad \text{for } 0.5 \leqslant \frac{r_b}{d_{bs}} \leqslant 1.0 \\ &= 0.17 \quad \text{for } 1.0 < \frac{r_b}{d_{bs}} \leqslant 1.5 \end{aligned} \tag{22b}$$

The expressions for d_{bs}, r_b and θ_b are already given by Eqs. (18), (19f) and (20b), respectively. Using the above procedure the pressure drop for the flow stream bend in the window section has been determined in simplified manner.

Now the pressure drop in window zone is given by Eq. (23), which is the summation of Eqs. (13b) and (21a).

$$\Delta p'_{wz} = \Delta p_{cdn} + \Delta p_b \quad \text{or}$$

$$\Delta p'_{wz} = \rho_s u_{sc}^2 f_1 \left[\left(\frac{A_{sc}}{A_{wz}}\right)^2 - 1\right]\left(\frac{\mu_{sw}}{\mu_s}\right)^{0.14} + \frac{\rho_s k u_{wz}^2}{2} \tag{23}$$

As discussed above in developing $\Delta p'_{wz}$, we have considered some approximations. Further it is also a fact that the baffle spacing changes flow pattern. The optimum ratio of baffle spacing [19] to shell inside the diameter should lie between 0.3 and 0.6. However in heat exchangers, for which experimental results are used for comparing the model results, these ratios are different. In view of this a correction factor (B_s/D_s) has been introduced which has improved the model results. The final equation of Δp_{wz} is given by Eqs. (24).

$$\Delta p_{wz} = \Delta p'_{wz} \times \frac{B_s}{D_s} \quad \text{or} \tag{24a}$$

$$\Delta p_{wz} = \frac{2\rho_s u_{sc}^2 f_i B_s}{2D_s}\left[\left(\frac{A_{sc}}{A_{wz}}\right)^2 - 1\right]\left(\frac{\mu_{sw}}{\mu_s}\right)^{0.14} + \frac{\rho_s k u_{wz}^2 B_s}{2D_s} \tag{24b}$$

The total pressure drop in the interior compartments is determined using Eqs. (12) and (24b) and given by Eq. (24c).

$$\Delta p_{ic} = (N_b - 1)\Delta p_c + N_b \Delta p_{wz} \tag{24c}$$

2.3. Pressure drop in end cross-sections due to fluid flow across the tube bundle

The end cross flow sections are those parts of the heat exchanger shell, which lie between one of the tube plates and the adjacent baffle (Fig. 7). The inlet and outlet cross flow sections do not have leakage streams that flow in a following cross flow sections. Therefore the influence of leakage in inlet and outlet cross flow sections is not considered. On the basis of this argument, the inlet and outlet sections are affected by bypass stream but not by leakage. Additionally there is an effect due to variable baffle spacing at the inlet and outlet sections of the shell. In addition, we observe the flow direction in the inlet and outlet regions, more or less perpendicular to the tube bundle and therefore there is no need to consider inclined direction of flow. On the basis of discussion given here to compute the pressure loss at inlet and outlet sections the expression given in Ref. [12] has been used in the present work, which is given here by Eq. (25a).

$$\Delta p'_{ec} = \frac{\rho_s f u_{sc}^2}{2} N_c \left(1 + \frac{N_w}{N_c}\right) f_b f_s \left(\frac{\mu_{sw}}{\mu_s}\right)^{0.14} \tag{25a}$$

The values of N_w, N_c, f_b and f_s have been computed using the expressions given by Taborek [8]. For both the end sections, the total pressure drop Δp_{ec} is obtained after multiplying $\Delta p'_{ec}$ by 2 and finally is given by Eq. (25b).

$$\Delta p_{ec} = 2\Delta p'_{ec} \tag{25b}$$

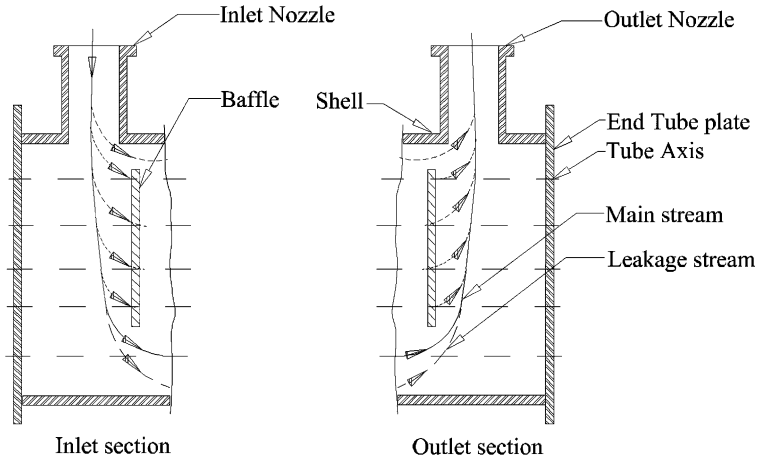

Fig. 7. Leakages at inlet and outlet sections.

Table 2
Giving the summary equations of various pressure drop components

Pressure drop in the inlet and outlet nozzles	$\Delta p_n = \rho_s u_n^2$
Pressure drop in the one interior cross flow section	$\Delta p_c = \frac{\rho_s f u_{sc}^2 N_c}{2\sin\theta} f_i f_b \left(\frac{\mu_{sw}}{\mu_s}\right)^{0.14}$
Pressure drop in one window zone	$\Delta p_{wz} = \frac{2\rho_s u_{sc}^2 f_i B_s}{2D_s}\left[\left(\frac{A_{sc}}{A_{wz}}\right)^2 - 1\right]\left(\frac{\mu_{sw}}{\mu_s}\right)^{0.14} + \frac{\rho_s k u_{wz}^2 B_s}{2D_s}$
Pressure drop in inlet or outlet end cross flow section	$\Delta p_{ec} = \rho_s f u_{sc}^2 N_c \left(1 + \frac{N_w}{N_c}\right) f_b f_s \left(\frac{\mu_{sw}}{\mu_s}\right)^{0.14}$

Table 3
Comparison of model and experimental results

Heat exchanger configuration				Flow rate (m^3/s) $\dot{V}$	Reynolds number Re_s	Exp. pressure (kpa) Δp_{Exp}	Present model pressure (kpa) Δp_{Model}	Percentage error compared to experimental results				
Cross passes #	Nozzle diameter (m)	Tube configuration (degrees)	Baffle cut (%)					Present model	HEATX [22]	Taborek [8]	Gaddis [18]	Kern [1]
Halle [13]												
6	0.337	30	29.0	0.080	23,733	36.32	35.20	−03.1	−06.3	04.1	14.8	19.2
6	0.337	30	29.0	0.100	29,667	55.13	54.35	−01.4	−05.6	05.8	15.4	18.1
6	0.337	30	29.0	0.120	35,600	77.53	77.53	00.0	−07.1	07.2	16.0	17.2
6	0.337	30	29.0	0.133	39,457	93.97	94.73	00.8	−07.4	08.0	16.3	16.2
8	0.337	30	26.0	0.133	52,579	157.75	161.62	02.4	−03.1	20.1	28.0	37.6
6	0.241	30	29.0	0.133	39,457	107.65	103.55	−03.9	02.8	09.5	09.2	04.6
6	0.337	45	30.0	0.050	10,765	10.19	09.79	−04.0	–	01.5	10.4	22.9
8	0.241	90	26.0	0.215	82,010	339.99	348.19	02.3	–	19.5	27.5	18.1
8	0.241	90	26.0	0.262	1,00,014	498.68	510.41	02.3	–	19.7	27.9	16.0
Bergelin [3]												
6	0.096	30	17.56	0.0018	1,001	1.67	1.69	01.1	–	46.7	58.4	83.1
6	0.096	30	17.56	0.0024	1,298	2.63	2.69	02.2	–	47.9	61.6	83.2
6	0.096	30	17.56	0.0033	1,785	5.07	5.19	02.3	–	45.5	61.3	82.1
6	0.096	30	17.56	0.0048	2,575	8.61	8.42	−02.2	–	53.6	67.3	84.3
6	0.096	30	17.56	0.0075	3,977	19.63	19.73	00.5	–	53.4	66.3	83.7
6	0.096	30	17.56	0.0120	6,545	51.80	52.41	01.1	–	52.0	63.7	82.5

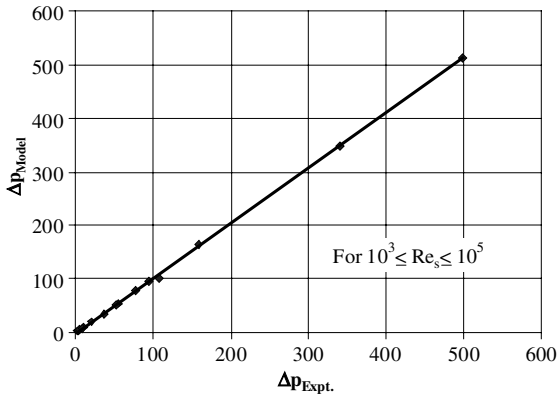

Fig. 8. Comparison of present model and Halle [13] and Bergelin [3] experimental results for shell-side pressure drop (kpa).

2.4. Total pressure drop in the shell

All these pressure drop components Δp_n, Δp_c, Δp_{wz} and Δp_{ec} are summarized in Table 2. The total pressure drop is given by Eq. (26).

$$\Delta p_s = \Delta p_n + (N_b - 1)\Delta p_c + N_b \Delta p_{wz} + \Delta p_{ec} \quad (26)$$

$$N_b = \frac{l - B_{si} - B_{so}}{B_s} + 1 \quad (27)$$

3. Comparison of the present model results with those available in the literature

The comparison of present model results has been done with experimental results [3,13] and results of the models developed by others [1,8,18,22]. This comparison is shown in Table 3. The total Reynolds numbers range covered, lies between 10^3 and 10^5. The comparison of model results with the experimental results has also been shown in Fig. 8. The present model results for water and oil fluids in the shell match with experimental results quite closely and the percentage error lies within +2.4% to −4.0%. The comparison of results determined by Prithiviraj et al. [22] for water flow in the shell using HEATX simulation with the experimental results [3] for Reynolds numbers ranging from 23,000 to 52,000 lie within +2.8% to −7.4%. Further the comparison of literature model results [1,8,18] with experimental results of Bergelin [3] and Halle [13] shows much higher errors as shown in Table 3. It would be worth to mention that the present model results compare well with experimental results for the fluids, water [13] and oil [3] flowing on the shell-side. This shows that the results of the present model match more closely with the experimental results compared to other models available in literature.

4. Conclusions

The present model is developed based on estimated actual flow pattern of the liquid in the shell. The model is simple and based on geometrical and operating parameters of the heat exchanger and covers the Reynolds numbers

ranging from 10^3 to 10^5. The present model results can be used by designers confidently.

References

[1] D.Q. Kern, Process Heat Transfer, Mc-Graw-Hill, New York, 1950, pp. 127–171.

[2] T. Tinker, N.Y. Buffalo, Shell-side characteristics of shell-and-tube heat exchangers: a simplified rating system for commercial heat exchangers, Trans. ASME (Jan.) (1958) 36–52.

[3] O.P. Bergelin, K.J. Bell, M.D. Leighton, Heat Transfer and Fluid Friction During Flow Across Banks of Tubes-VI, Trans. ASME (Jan.) (1958) 53–60.

[4] W.H. Emerson, Shell-side pressure drop and heat transfer with turbulent flow in segmentally baffled shell-tube heat exchangers, Int. J. Heat Mass Transfer 6 (1963) 649–668.

[5] W.J. Duncan, A.S. Thom, A.D. Young, Mechanics of Fluids, Edward Arnold (Publishers) Ltd., London, 1970, pp. 412–414.

[6] J.D. Jenkins, Single-phase coefficients on the shell-side of baffled heat exchangers, in: D. Chisholm (Ed.), Developments in Heat Exchanger Technology, 1980, pp. 11–53.

[7] E.M. Sparrow, J.A. Parez, Internal, shell-side heat transfer and pressure drop characteristics for a shell and tube heat exchanger, J. Heat Transfer 107 (1985) 345–353.

[8] R.K. Shah, A.C. Mueller, Process heat exchangers, in: Handbook of Heat Transfer Applications, 1985, pp. 80–173.

[9] E.M. Sparrow, L.G. Reifschneider, Effect of inter baffle spacing on heat transfer and pressure drop in a shell-and-tube heat exchanger, Int. J. Heat Mass Transfer 29 (11) (1986) 1617–1628.

[10] I.I. Ionel, Pumps and Pumping, Elsevier, Amsterdam, Oxford, New York, 1986, pp. 194–218.

[11] E.A.D. Saunders, Heat Exchangers, John Wiley & Sons, New York, 1988, pp. 43.

[12] K.J. Bell, Delware method for shell-side design, in: R.K. Shah, E.C. Subbarao, R.A. Mashelkar (Eds.), Heat Transfer Equipment Design, Hemisphere Publishing Corporation, 1988, pp. 145–166.

[13] H. Halle, J.M. Chenoweth, M.W. Wambsganss, Shell-side water flow pressure drop distribution measurements in an industrial-sized test heat exchanger, J. Heat Transfer 110 (1988) 60–67.

[14] R.S. Kistler, J.M. Chenoweth, Heat exchanger shell side pressure drop: comparison of predictions with experimental data, J. Heat Transfer 110 (1988) 68–76.

[15] A.P. Fraas, Heat Exchanger Design, John Wiley & Sons, 1988, pp. 228–245.

[16] T. Pekdemir, T.W. Davies, L.E. Haseler, A.D. Diaper, Flow distribution on the shell side of a cylindrical shell and tube heat exchanger, Int. J. Heat Fluid Flow 14 (1) (1993) 76–85.

[17] T. Pekdemir, T.W. Davies, L.E. Haseler, A.D. Diaper, Pressure drop measurements on the shell side of a cylindrical shell-and-tube heat exchanger, J. Heat Transfer 15 (3) (1994) 42–55.

[18] E.S. Gaddis, V. Gnielinski, Pressure drop on the shell side of shell-and-tube heat exchangers with segmental baffles, Chem. Eng. Process. 36 (1997) 149–159.

[19] R. Mukherjee, Effectively design shell-and-tube heat exchangers, Chem. Eng. Prog. 2 (1998).

[20] M. Prithiviraj, M.J. Andrews, Three-dimensional numerical simulations of shell-and-tube heat exchangers. Part I: Foundation and fluid mechanics, Numer. Heat Transfer. Part A 33 (1998) 799–816.

[21] H. Li, V. Kottke, Effect of baffle spacing on pressure drop and local heat transfer in shell-and-tube heat exchangers for staggered tube arrangement, Int. J. Heat Mass Transfer 41 (10) (1998) 1303–1311.

[22] M. Prithiviraj, M.J. Andrews, Comparison of a three-dimensional numerical model with existing methods for prediction of flow in shell-and-tube heat exchangers, Heat Transfer Eng. 20 (2) (1999) 15–19.

[23] S. Kakac, H. Liu, Heat Exchangers Selection, Rating and Thermal Design, CRC press, Washington D.C., 2002, pp. 318–335.